Direct observation of double hydrogen transfer via quantum tunneling in a single porphycene molecule on a Ag(110) surface

Matthias Koch[1], Mark Pagan[2], Mats Persson[2], Sylwester Gawinkowski[3], Jacek Waluk[3, 4], and Takashi Kumagai*[1]

[1]Department of Physical Chemistry, Fritz-Haber Institute of the Max-Planck Society, Faradayweg 4-6, 14195 Berlin, Germany.

[2]Surface Science Research Centre and Department of Chemistry, University of Liverpool, Liverpool L69 3BX, UK.

[3]Institute of Physical Chemistry, Polish Academy of Sciences, Kasprzaka 44/52, Warsaw 01-224, Poland.

[4]Faculty of Mathematics and Natural Sciences, College of Science, Cardinal Stefan Wyszyński University, Dewajtis 5, 01-815 Warsaw, Poland

*corresponding author: kuma@fhi-berlin.mpg.de

ABSTRACT

Quantum tunneling of hydrogen atoms (or proton) plays a crucial role in many chemical and biological reactions. Although tunneling of a single particle has been examined extensively in various one-dimensional potentials, many-particle tunneling in high-dimensional potential energy surfaces remains poorly understood. Here we present a direct observation of a double hydrogen atom transfer (tautomerization) within a single porphycene molecule on a Ag(110) surface using a cryogenic scanning tunneling microscope (STM). The tautomerization rates are temperature-independent below ~10 K and a large kinetic isotope effect (KIE) is observed upon substituting the transferred hydrogen atoms by deuterium. The observed KIE for three isotopologues and density functional theory calculations indicate that a stepwise transfer mechanism is dominant in the tautomerization. It is also found that the tautomerization rate is increased by vibrational excitation via an inelastic electron tunneling process. Moreover, the STM tip can be used to manipulate the tunneling dynamics through modification of the potential landscape.

INTRODUCTION

Hydrogen-transfer reactions are involved in a variety of chemical and biological processes.[1] As being the lightest element, the hydrogen atom is subject to important nuclear quantum effects (NQEs),[2, 3, 4, 5] leading to peculiar static and dynamic properties which cannot be rationalized by classical mechanics. For instance, already in 1927 the importance of quantum tunneling was pointed out by Hund for an intramolecular hydrogen rearrangement such as flipping of ammonia (umbrella motion).[6] Tunneling is not only of fundamental interest in quantum physics/chemistry but also plays a crucial role in important chemical[7, 8] and enzymatic[9] reactions. Although single-particle tunneling has been well-studied in various types of one-dimensional potentials,[10] the accurate description of many-particle tunneling in a multi-dimensional potential energy surface is far from complete. Additionally, intermolecular interactions or crystal fields could affect the tunneling dynamics in condensed phases, but it remains a challenging task to probe directly NQEs at the single-molecule level. Recently low-temperature STM has been proven to be a novel and powerful tool to investigate NQEs of hydrogen on surfaces *in real space*, whereby hydrogen diffusion,[11] hydrogen-bond rearrangement in small water clusters[12, 13] and flipping motion of hydrogen atom[14] via tunneling, and the zero-point energy contribution in the hydrogen bond[15, 16] were directly observed.

Additionally, theoretical calculations also highlighted considerable impacts of NQEs on the structure and dynamics of adsorbed molecules.[17, 18, 19] Interestingly, tunneling was found to be an important contribution to hopping (diffusion) of heavy atoms and molecules such as Cu,[20] Co,[21] and CO[22] on a Cu(111) surface at cryogenic temperatures.

In a multiple hydrogen (proton) transfer, the process occurs either in a stepwise or concerted fashion. In the former case, individual hydrogen atoms move separately and there exist multiple transition states and meta-stable intermediate structures along the reaction pathway. In the latter case, the hydrogen atoms are transferred collectively and the reaction coordinate exhibits a single transition structure. Tautomerizations in porphyrins and phthalocyanines have served as fascinating models to study double hydrogen transfer reactions.[1] Recently low-temperature STM has been employed to investigate tautomerization in a single molecule adsorbed on surfaces.[23, 24, 25] These pioneering studies proposed that tautomerization could be exploited to make a single-molecule switching device in future molecular electronics. Porphycene, the first synthesized constitutional isomer of porphyrin,[26] has emerged as an intriguing model for intramolecular hydrogen bonding and a double hydrogen transfer.[27, 28] Because of the strong intramolecular hydrogen bonds, the potential landscape of tautomerization in porphycene is significantly shallower as compared to porphyrins and phthalocyanines,

leading to pronounced NQEs that is hydrogen tunneling.[29] Porphycene occurs as the *trans* or *cis* tautomer (**Fig. 1a**) with comparable total energies within only a few kcal/mol (Ref. 30 and see our calculated results in Supporting Information). In the gas phase, *trans–trans* tautomerization takes place via coherent tunneling and its rate was estimated to be 6×10^{11} Hz from the tunneling splitting (4.4 cm^{-1}) of the vibronic levels at the ground state.[31] A crucial role of tunneling, even at room temperature, was also found in the condensed phase.[32] Because the barrier heights of the stepwise and concerted pathway were also estimated to be comparable, it was proposed that the tautomerization might take place in a competing manner.[33] Additionally, the tautomerization coordinate of porphycene is essentially multi-dimensional and several vibrational modes act as a reaction-promoter or inhibitor through anharmonic intermode coupling.[31] However, the tunneling process was found to be quenched upon adsorption on a Cu(110) surface due to the interaction of the porphycene with the surface atoms.[34, 35] Here we present that tautomerization of porphycene occurs via tunneling on a less reactive Ag(110) surface and elucidate the reaction mechanism by a combination of low-temperature STM experiments and density functional theory (DFT) calculations.

METHODS

Experiments were carried out under ultrahigh vacuum conditions (<2×10^{-10} mbar) with a low-temperature STM from Omicron Nanotechnology GmbH and operated with Nanonis Controller System from Specs GmbH. An electrochemically etched Au tip was used as a STM probe. The bias voltage (V_{bias}) was applied to the sample and the tip was grounded. A single-crystalline Ag(110) surface was cleaned by repeated cycles of argon ion sputtering and annealing to 670 K. We investigated three isotopologues, namely HH-, HD-, and DD-porphycene. In the latter two species, the inner hydrogen atoms within the molecular cavity are replaced by one or two deuterium atoms. The deuteration was carried out by repeated recrystallization cycles with CD_3OD/CD_2Cl_2 solution.[36] The partially deuterated species, HD-porphycene, is involved as an impurity in the deuteration process of the parent HH-porphycene and its existence was established by high-resolution electronic spectroscopy with ultra-cold molecules isolated in helium nanodroplets.[31] We used a deuterated sample that contains HD-species. The purity of the sample used was checked under UHV conditions by depositing the sample onto a Cu(110) surface where each species can be discriminated by single-molecule vibrational spectroscopy of the STM (see Supporting Information for details of the identification). Porphycene molecules were evaporated from a

Knudsen cell at ~450 K while the Ag(110) sample was kept at room temperature.

The geometric structures and the minimum energy paths (MEPs) of the adsorbed porphycene on the Ag(110) surface were obtained from periodic, plane-wave DFT calculations using the Vienna *ab-initio* simulation program (VASP).[37] The electron–ion core interactions and the exchange–correlation effects were treated using the Projector Augmented Wave (PAW) method[38] and the optB86B version of the van der Waals density functional,[39, 40, 41, 42] respectively. The robustness of the calculated results was investigated using the BEEF-vdW[43] and the vdW-DF-cx functionals.[44] The Ag(110) surface was represented in a super-cell by a four layer slab with a 4×6 surface unit cell and a 20 Å vacuum region. The MEPs were computed with the nudged elastic band method.[45, 46] Further details of the calculations can be found in the Supporting Information.

RESULTS AND DISCUSSION

Figure 1b displays topographic STM images of a single porphycene molecule on Ag(110) at 5 K. The crescent-shaped appearance is similar to that on Cu(110)[35] and indicates that the porphycene adsorbs in the *cis* configuration. Our DFT calculations also predict the *cis* configuration to be the most stable tautomer on Ag(110) (**Fig. 1c**),

although the relative energy difference $\Delta E_{cis-trans}$ is quite small (0.023 eV). The brighter side in the topographic image of the porphycene (**Fig. 1b**) corresponds to the side where two hydrogen atoms are bonded to the pyrrole nitrogen atoms.[35] In the gas phase, solution, or crystalline state, the *trans* configuration has been observed to be the most stable tautomer. However, the preference of the *cis* configuration on the Ag(110) surface could be explained by a strong interaction between the amine nitrogen atoms (with a lone pair) in the molecular cavity and the surface atoms underneath, which form dative bonds. The adsorption also causes a slight deformation of the porphycene macrocycle that is fully planar in the gas phase. Our calculations unveil that this deformation makes the *trans* configuration even more preferable than the *cis* configuration in the absence of the surface (see Supporting Information). Thus, the stabilization of the *cis* tautomer on the surface is not caused by the buckling but is caused by the molecule–surface interaction.

It is found that the porphycene switches between two orientations as shown in **Fig. 1b**, which corresponds to the *cis* ↔ *cis* tautomerization through a double hydrogen transfer within the molecular cavity. Interestingly, this reaction occurs spontaneously even at 5 K and exhibits a strong isotope effect. **Figure 1d** shows an STM image of normal and deuterated species (HH- and DD-porphycene, respectively). The rapid

tautomerization rate of HH-porphycene is reflected by its fluctuating image, whereas the rate is much smaller for DD-porphycene and only a single tautomerization event is observed in **Fig. 1d**, thus revealing a large kinetic isotope effect (KIE). Additionally, in the course of the *cis* ↔ *cis* tautomerization we find experimentally a small translational motion of the molecule along the [001] direction (**Fig. 1b**), which is also confirmed in the calculated structure (**Fig. 1c**). This displacement is clearly visible in the DD-porphycene of **Fig. 1d**.

The observed KIE indicates the dominant contribution of tunneling to tautomerization, as is further confirmed by investigating the dependence of the tautomerization rate on the tunneling current, the bias voltage, and the temperature. Tautomerization of an individual porphycene was directly monitored by tracing the change in the tip height over the molecule (**Fig. 2a**) while fixing the lateral tip position, as indicated by the markers in **Fig. 1d**. The tautomerization results in a random telegraph signal where the "high" and "low" states correspond to the configurations such that the inner hydrogen atoms locate close to and away from the tip, respectively (see schematics in **Fig. 2b** and **c**). The change in the tip height of about 0.2 Å corresponds to the difference in the topographic height of the brighter and the darker side of porphycene which correspond to the pyrrole rings with imine and amine nitrogen

atoms, respectively. For DD-porphycene an additional level (a third state) can be observed in the tip height trace, which appears intermittently in between the "high" and "low" states (**Fig. 2d**). This state should be attributed to the meta-stable *trans* configuration (as discussed below). However, this short-lived *trans* state was not observed for HH-porphycene most probably due to the limited time-resolution of the STM (few milliseconds in the measurement used) which is not sufficient to capture it. **Figure 2e** shows the current dependence of the tautomerization rate for HH-porphycene at a fixed bias voltage ($R_{H\rightarrow L}$ and $R_{L\rightarrow H}$ denote the rate from "high" to "low" transition and the reverse process, respectively). $R_{H\rightarrow L}$ and $R_{L\rightarrow H}$ show a rather weak dependence on the current below ~0.2 nA, indicating that tunneling electrons, an electric field, and the tip–molecule interaction do not play a significant role (the similar behavior was also confirmed for the other isotopologues, see Supporting Information). However, $R_{H\rightarrow L}$ and $R_{L\rightarrow H}$ clearly deviate from each other at higher currents, which should be ascribed to the deformation of the tautomerization potential energy surface, caused by the tip–molecule interaction upon tip approach (*cf.* **Fig. 4**). **Figure 2f** shows the bias voltage dependence of the tautomerization rate measured at a fixed tunneling current (5 pA). The tautomerization rate rapidly increases above 50 mV for all isotopologues. At lower voltages, the rate shows a slight increase, which should be attributed to the proximity of

tip–molecule distance. The voltage-dependent rate appears symmetric at both bias polarities and the thresholds of the rate increase are similar for all isotopologues. The HOMO–LUMO gap of porphycene is about 2 eV[29] which does not match the energy range of the threshold voltages (~50 mV). Therefore, the increase of the tautomerization cannot be attributed to the electronic excitation. However, it is likely that the threshold voltages represent vibrational excitation of a skeletal mode of porphycene which couples with the tautomerization coordinate.[31] Hence, we conclude that the increase of the rate occurs by vibrational excitation via an inelastic electron tunneling process.[34] In **Fig. 2f**, the voltage dependence for the three isotopologues (open markers) was obtained under the same tip conditions. However, the rate shows a variation (vertical offset) when it is measured under different tip conditions, *e.g.*, use of a different tip or execution of *in-situ* tip preparations like application of voltage pulse or tip indentation into the surface, as shown by the filled circles in **Fig. 2f**. The error bar of the rate in all presented data takes into account this experimental uncertainty.

The *cis* ↔ *cis* tautomerization via tunneling on Ag(110) is conclusive from the temperature-dependent rates (**Fig. 2g**). For all isotopologues, the rate is independent of the temperature below ~10 K and exhibits a large KIE of about 100 between HH- and DD-porphycene, while the KIE between DD- and HD-porphycene is about 2. The Bell–

Limbach tunneling model[47]—an accepted model to explain a temperature-dependent reaction rate of multiple hydrogen (proton) transfers including tunneling at low temperatures—revealed that the KIE of the rate constant, k_{LL}, (L = H or D) in the tunneling regime to be $k_{HH} \gg k_{HD} \cong 2k_{DD}$ or $k_{HH}/k_{HD} \approx k_{HD}/k_{DD}$ for the stepwise or concerted mechanisms, respectively.[48, 49, 50, 51] The theoretical calculations by Smedarchina and coworkers[52] corroborated these ratios of KIEs for the stepwise and concerted mechanisms for tautomerization of porphycene isotopologues using a quantum mechanical model with an approximate instanton method. In the stepwise mechanism, k_{HD} is expected to be close to k_{DD} because the deuterium transfer should be the rate-limiting step in the HD-species. On the other hand, k_{HD} should be closer to k_{HH} in the concerted mechanism than for the stepwise one. Our result is in line with the stepwise scenario and we assign the third state observed in the tip height trance for DD-porphycene (**Fig. 2d**) to the meta-stable *trans* configuration.

The reaction pathway and barrier are examined using DFT calculations. It is revealed that the stepwise mechanism (**Fig. 3a**) via the first-order saddle points and the meta-stable *trans* configuration shows a lower barrier than that of the concerted mechanism (**Fig. 3b**) via the second-order saddle point. The zero-point energy (ZPE) corrected barrier is calculated to be 0.064(0.103) eV and 0.094(0.172) eV for the

stepwise and concerted pathway, respectively (values within parentheses refer to DD-porphycene). In either case, the barrier cannot be overcome through thermal activation at 5 K, corroborating that the reaction is dominated by tunneling. Thus, the stepwise pathway is more likely than the concerted one in terms of the barrier height, which is consistent with experiment. On the other hand, the barrier width (transition path length) may also influence the tunneling process. However, it is not feasible to extract the contribution of the path length in a quantitative manner when the motion of heavy atoms is involved.[19] In the case of the porphycene on Ag(110), we found the significant displacement of carbon and nitrogen atoms upon the *cis* ↔ *cis* tautomerization (*cf.* **Fig. 1**), making it extremely difficult to determine the tunneling pathway and consequently estimate the tunneling rate.

The tautomerization rate via tunneling on Ag(110) is considerably reduced compared to the rate in the gas phase (6×10^{11} Hz for HH-porphycene[31]). This reduction is explained by an increase of the tautomerization barrier as compared to 0.023(±0.002) eV estimated for the *trans* ↔ *trans* tautomerization in inert media.[29] Additionally, symmetry lowering of the porphycene due to adsorption may also play a role; the increase of the path length due to the motion of the porphycene during tautomerization results may reduce the tunneling rate.[19] This is in contrast to the gas phase where the

tautomerization coordinate is dominated predominantly by the motion of the inner hydrogen atoms. Moreover, the calculated structure (inset of **Fig. 3b**) revealed a slight deformation of the porphycene macrocycle, resulting from a stronger interaction of the amine nitrogen atoms with the surface Ag atoms than the imine nitrogen atoms. This molecule–surface interaction stabilizes the *cis* configuration over the *trans* configuration but gives rise to an increase of the tautomerization barrier. It should be noted that no spontaneous tautomerization (via tunneling) was observed for the porphycene on Cu(110) at 5 K, although tautomerization can be induced by the STM through an inelastic electron tunneling process.[34, 35] The absence of the tunneling process can be rationalized by the stronger molecule–surface interaction on Cu(110) than that on Ag(110), as implied by a larger deformation of the molecular skeleton on Cu(110) (see Supporting Information). The tautomerization barrier of HH-porphycene on Cu(110) is calculated to be 0.20 and 0.35 eV for the stepwise and concerted mechanism, respectively, which are larger than Ag(110) (see Supporting Information). This increase of the barrier is found to be robust to the choice of exchange–correlation functional (see Supporting Information).

The local environment of a molecule can also strongly influence tunneling dynamics. We found that the tunneling rate (**Fig. 2e**) and the population of “high” and

"low" state (**Fig. 4a**), thus the kinetics of the *cis* ↔ *cis* tautomerization on Ag(110), can be manipulated by varying the tip–molecule distance. The tautomerization is eventually quenched when the tip was brought close to the molecule. **Figure 4b** shows the populations of the "low" and "high" states obtained under two different tip conditions (the tip apex structure was changed by a controlled indentation of the tip into the surface) and with a CO-modified tip. Although the variation of the rate and population also depends on the tip conditions, the general tendencies remain similar. The increasing population of the "high" state with decreasing the tip–molecule distance suggests that an attractive interaction between tip and molecule makes the "high" state more preferable as schematically shown in **Fig. 4c**. Our recent study[53] has demonstrated that the symmetric potential energy surface of the *cis* ↔ *cis* tautomerization on Cu(110) can be deformed in the presence of the tip such that the "high" state becomes more favorable than the "low" state in the attractive force regime, whereas their relative stability reverses in the repulsive regime. Because the tip–molecule distance in **Fig. 4b** is expected to be relatively large, the interaction stays in the attractive force regime which should lead to preference of the "high" state.

CONCLUSION

A double hydrogen transfer (*cis* ↔ *cis* tautomerization) via tunneling was observed directly in single porphycene molecules on a Ag(110) surface using a low-temperature STM. The dominant contribution of tunneling was manifested as temperature-independent tautomerization rate below ~10 K. Additionally, the short-lived *trans* state observed for DD-porphycene, the isotope ratio of the tautomerization rate between different isotopologues, and the DFT calculations indicated that the tautomerization occurs by the stepwise mechanism rather than the concerted one. The DFT calculations also revealed the stable adsorption structure of the porphycene on Ag(110) and MEPs of the *cis* ↔ *cis* tautomerization. The planar macrocycle of porphycene in the gas phase was found to be deformed upon adsorption but the *cis* configuration is stabilized by the strong interaction between the amine nitrogen atoms in the molecular cavity and the Ag atoms underneath. The calculated barrier of 0.064 eV for the stepwise pathway was too large to be overcome at cryogenic temperatures, corroborating that the tautomerization is governed by tunneling. It was also found that the vibrational excitation of a skeletal mode via an inelastic electron tunneling process increases the tautomerization rate. Moreover, the tunneling dynamics could be manipulated by varying the tip–molecule distance (interaction) which modifies the potential energy surface and changes the

tunneling rate (eventually quenches the reaction). We believe that our results represent a benchmark experiment for examining a double hydrogen transfer via tunneling in multi-dimensional potential energy surfaces with high level of theoretical simulations.

ASSOCIATED CONTENT

Supporting Information

The Supporting Information is available free of charge on the ACS Publications website.

AUTHOR INFORMATION

Corresponding Author

kuma@fhi-berlin.mpg.de

Author Contributions

Notes

The authors declare no competing financial interests.

ACKNOWLEDGMENT

The authors thank Mariana Rossi and Martin Wolf for stimulating discussions. T.K. acknowledges the support of Morino Foundation for Molecular Science. M.P. acknowledges computer time allocated on ARCHER through the Materials Chemistry Consortium (EPSRC grant no. EP/L000202), on Polaris through N8 HPC (EPSRC grant no. EP/K000225/1) and on Chadwick at the University of Liverpool. J.W. acknowledges the grant from the Polish National Science Centre (DEC-2013/10/M/ST4/00069).

References

[1] Hynes, J. T.; Klinman, J. P.; Limbach, H.-H.; Schowen, R. L. *Hydrogen-Transfer Reactions.* Wiley-VCH, **2007**.

[2] Tuckerman, M. E.; Marx, D.; Klein, M. L.; Parrinello, M. *Science* **1997**, *275*, 817.

[3] Tuckerman, M. E.; Marx, D.; Parrinello, M. *Nature* **2002**, *417*, 925.

[4] Li, X.-Z.; Walker, B.; Michaelides, A. *Proc. Natl. Acad. Sci. U.S.A.* **2010**, *108*, 6369.

[5] Ceriotti, M.; Fang, W.; Kusalik, P. G.; McKenzie, R. H.; Michaelides, A.; Morales, M. A.; Markland, T. E. *Chem. Rev.* **2016**, *116*, 7529.

[6] Hund, F. *Z. Phys.* **1927**, *43*, 803.

[7] McMahon, R. J. *Science* **2003**, *299*, 833.

[8] Shannon, R. J.; Blitz, M. A.; Goddard, A.; Heard, D. E. *Nat. Chem.* **2013**, *5*, 745.

[9] Klinman, J. P.; Kohen, A. *Annu. Rev. Biochem.* **2013**, *82*, 471.

[10] Bell, R. P. *The Tunneling Effect in Chemistry.* Chapman and Hall, **1980**.

[11] Lauhon, L. J.; Ho, W. *Phys. Rev. Lett.* **2000**, *85*, 4566.

[12] Kumagai, T.; Kaizu, M.; Hatta, S.; Okuyama, H.; Aruga, T.; Hamada, I.; Morikawa, Y. *Phys. Rev. Lett.* **2008**, *100*, 166101.

[13] Kumagai, T.; Kaizu, M.; Okuyama, H.; Hatta, S.; Aruga, T.; Hamada, I.; Morikawa, Y. *Phys. Rev.* B **2010**, *81*, 045402.

[14] Kumagai, T.; Kaizu, M.; Okuyama, H.; Hatta, S.; Aruga, T.; Hamada, I.; Morikawa, Y. *Phys. Rev.* B **2009**, *79*, 035423.

[15] Meng, X.; Guo, J.; Peng, J.; Chen, J.; Wang, Z.; Shi, J.-R.; Li, X.-Z.; Wang, E.-G.; Jiang, Y. *Nat. Phys.* **2015**, *11*, 235.

[16] Guo, J.; Lü, J.-T.; Feng, Y.; Chen, J.; Peng, J.; Lin, Z.; Meng, X.; Wang, Z.; Li, X.-Z.; Wang, E.-G.; Jiang, Y. *Science* **2016**, *352*, 321.

[17] Ranea, V. A.; Michaelides, A.; Ramírez, R.; de Andres, P. L.; Vergés, J. A.; King, D. A. *Phys. Rev. Lett.* **2004**, *92*, 136104.

[18] Li, X.-Z.; Probert, M. I. J.; Alavi, A.; Michaelides, A. *Phys. Rev. Lett.* **2010**, *104*, 066102.

[19] Davidson, E. R. M.; Alavi, A.; Michaelides, A. *Phys. Rev.* B **2010**, *81*, 153410.

[20] Repp, J.; Fölsch, S.; Meyer, G.; Rieder, K.-H. *Phys. Rev. Lett.* **2003**, *91*, 206102.

[21] Stroscio, J. A.; Celotta, R. J. *Science* **2004**, *306*, 242.

[22] Heinrich, A. J.; Lutz, C. P.; Gupta, J. A.; Eigler, D. M. *Science* **2002**, *298*, 1381.

[23] Liljeroth, P.; Repp, J.; Meyer, G. *Science* **2007**, *317*, 1203.

[24] Sperl, A.; Kröger, J.; Berndt, R. *Angew.Chem. Int. Ed.* **2011**, *50*, 5294.

[25] Auwärter, W.; Seufert, K.; Bischoff, F.; Ecija, D.; Vijayaraghavan, S.; Joshi, S.; Klappenberger, F.; Samudrala, N.; Barth, J. V. *Nat. Nanotech.* **2012**, *7*, 41.

[26] Vogel, E.; Köcher, M.; Schmickler, H.; Lex, J. *Angew. Chem. Int. Ed.* **1986**, *25*, 257.

[27] Waluk, J. *Chem. Rev.* **2017**, *117*, 2447.

[28] Fita, P.; Grill, L.; Listkowski, A.: Piwonski, H.; Gawinkowski, S.; Pszona, M.; Sepiol, J.; Mengesha, E. T.; Kumagai, T.; Waluk, J. *Phys. Chem. Chem. Phys.* **2017**, 19, 4921.

[29] Waluk, J. *Acc. Chem. Res.* **2006**, *39*, 945.

[30] Yoshikawa, T.; Sugawara, S.; Takayanagi, T.; Shiga, M.; Tachikawa, M. *Chem. Phys. Lett.* **2010**, *496*, 14.

[31] Vdovin, A.; Waluk, J.; Dick, B.; Slenczka, A. *Chem. Phys. Chem.* **2009**, *10*, 761.

[32] Ciąćka, P.; Fita, P.; Listkowski, A.; Radzewicz, C.; Waluk, J. *J. Phys. Chem. Lett.* **2016**, *7*, 283.

[33] Yoshikawa, T.; Sugawara, S.; Takayanagi, T.; Shiga, M.; Tachikawa, M. *Chem. Phys.* **2012**, *394*, 46.

[34] Kumagai, T.; Hanke, F.; Gawinkowski, S.; Sharp, J.; Kotsis, K.; Waluk, J.; Persson, M.; Grill, L. *Phys. Rev. Lett.* **2013**, *111*, 246101.

[35] Kumagai, T.; Hanke, F.; Gawinkowski, S.; Sharp, J.; Kotsis, K.; Waluk, J.; Persson, M.; Grill, L. *Nat. Chem.* **2014**, *6*, 41.

[36] Fita, P.; Urbańska, N.; Radzewicz, C.; Waluk, J. *Z. Phys. Chem.* **2008**, *222*, 1165.

[37] Kresse, G.; Furthmüller, J. *Phys. Rev.* B **1996**, *54*, 11169.

[38] Kresse, G.; Joubert, D.; *Phys. Rev.* B **1999**, *59*, 1758.

[39] Dion, M.; Rydberg, H.; Schröder, E.; Langreth, D. C.; Lundqvist, B. I.; *Phys. Rev. Lett.* **2004**, *92*, 246401.

[40] Román-Pérez, G.; Soler, J. M. *Phys. Rev. Lett.* **2009**, *103*, 096102.

[41] Klimeš, J.; Bowler, D. R.; Michaelides, A. *J. Phys. Cond. Matt.* **2010**, *22*, 022201.

[42] Klimeš, J.; Bowler, D. R.; Michaelides, A. *Phys. Rev.* B **2011**, *83*, 195131.

[43] Wellendorff, J. ; Lundgaard, K. T.; Møgelhøj, A.; Petzold, V.; Landis, D. D.; Nørskov, J. K.; Bligaard, T.; Jacobsen, K. W. *Phys. Rev.* B **2012**, *85*, 235149.

[44] Berland, K.; Hyldgaard, P. *Phys. Rev.* B **2014**, *89*, 035412.

[45] Mills, G.; Jónsson, H.; Schenter, G. K. *Surf. Sci.* **1995**, *324*, 305.

[46] Henkelman, G.; Uberuaga B. P.; Jónsson, H. A. *J. Chem. Phys.* **2000**, *113*, 9901.

[47] Limbach, H.-H.; Lopez, J. M.; Kohen, A. *Philos. Trans. R. Soc. Lond.* B **2006**, *361*, 1399.

[48] Limbach, H.-H. Chapter 6 in *Hydrogen-Transfer Reactions*. Wiley-VCH: Weinheim, **2007**, page 135 and references therein.

[49] Wehrle, B.; Limbach, H.-H. *Chem. Phys.* **1989**, *136*, 223.

[50] Klein, O.; Aguilar-Parrilla, F.; Lopez, J. M.; Jagerovic, N.; Elguero, J. Limbach, H.-H. *J. Am. Chem. Soc.* **2004**, *126*, 11718.

[51] Lopez, J. M.; Männle, F.; Wawer, I.; Buntkowsky, G.; Limbach, H.-H. *Phys. Chem. Chem. Phys.* **2007**, *9*, 4498.

[52] Smedarchina, Z.; Shibl, M. F.; Kühn, O.; Fernández-Ramos, A. *Chem. Phys. Lett.*

2007, *436*, 314.

[53] Ladenthin, J. N.; Frederiksen, T.; Persson, M.; Sharp, J. C.; Gawinkowski, S.; Waluk, J.; Kumagai, T. *Nat. Chem.* **2016**, *8*, 935.

Table of Contents Graphic

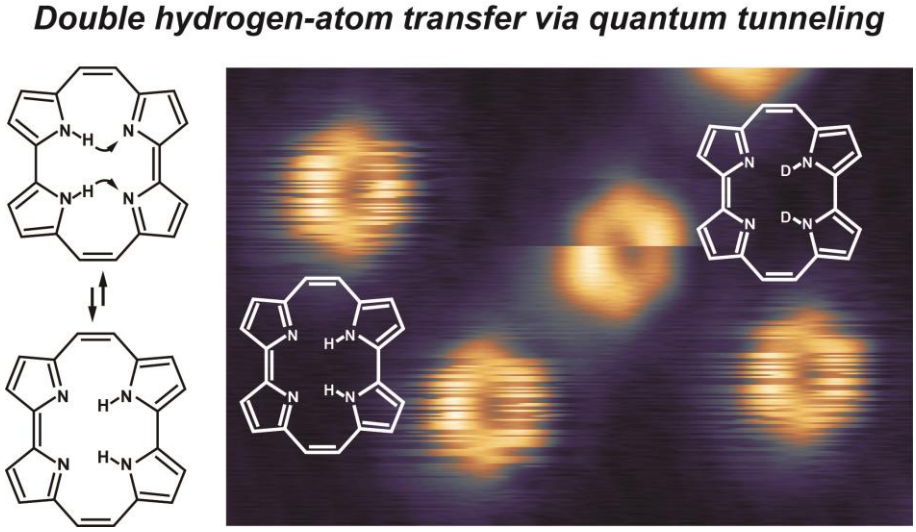

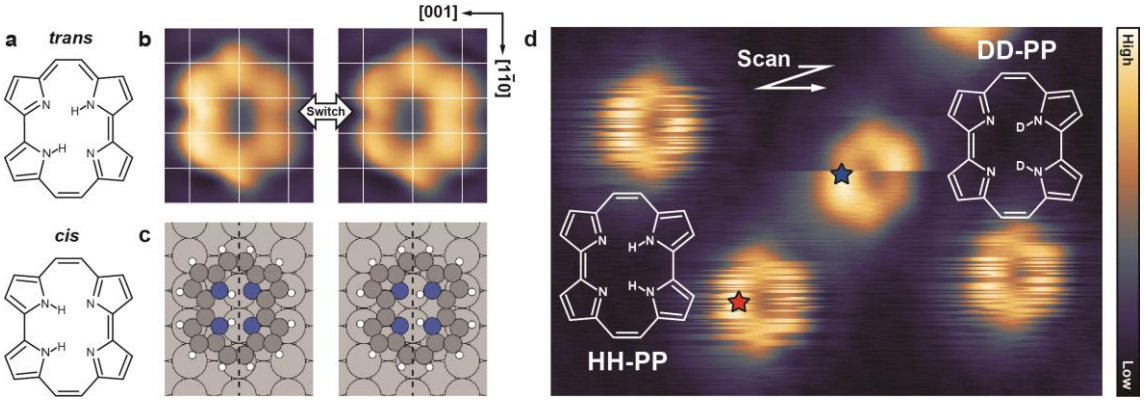

Figure 1. Porphycene molecule on Ag(110). a, Two tautomeric forms of porphycene. **b,** STM images of a single DD-porphycene molecule (5 K, V_{bias} = 50 mV, I_t = 0.1 nA, size: 1.6×2.0 nm^2). The white grid lines represent the surface lattice of Ag(110). **c,** Top view images of calculated *cis* structure and its mirror reflection. The dashed lines represent the high-symmetry (mirror) axis of the surface. **d,** STM image of HH- and DD-porphycene molecules (5 K, V_{bias} = 50 mV, I_t = 0.05 nA, size: 4.0×6.0 nm^2). The scanning direction is indicated by the white arrow.

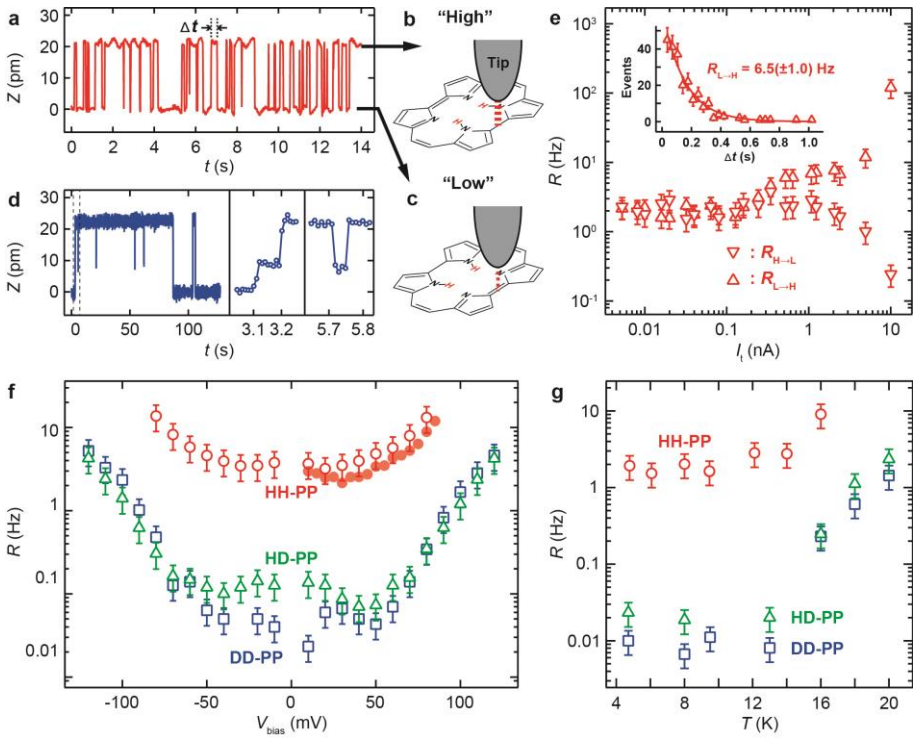

Figure 2. Dependence of tautomerization rate on tunneling current, temperature, and bias voltage. (a) Trace of tip height (Z) measured for HH-porphycene. The traces were acquired at a set current of 5 pA at V_{bias} = 30 mV. The lateral tip position during the measurement is indicated by the red and blue stars in **Fig. 1d**. (b) and (c) Schematic of "high" and "low" states. (d) Trace of tip height (Z) measured for DD-porphycene. The right panels show magnified Z traces marked by the dashed lines in the left, where a short-lived *trans* state is observed. (e) Current (I_t) dependence of the tautomerization rates for "high" to "low" ($R_{H\to L}$) at 5 K and the opposite process ($R_{L\to H}$) for HH-porphycene. V_{bias} was fixed to 20 mV during the measurement. The inset of shows a histogram of time intervals between tautomerization events (Δt) for the "low" to "high" process and measured at I_t of 0.63 nA. The rate is obtained to be 6.5(±1.0) Hz by fitting the data to an exponential decay function. (f) Voltage dependence of the total rate for HH-, HD-, and DD-porphycene measured at 5 K with I_t = 5 pA. The data of the open markers were obtained under the same tip conditions. The filled circles were obtained with a different tip. (g) Temperature (T) dependence of the tautomerization rate for HH-, HD-, and DD-porphycene measured at I_t = 10 pA and V_{bias} = 10 mV.

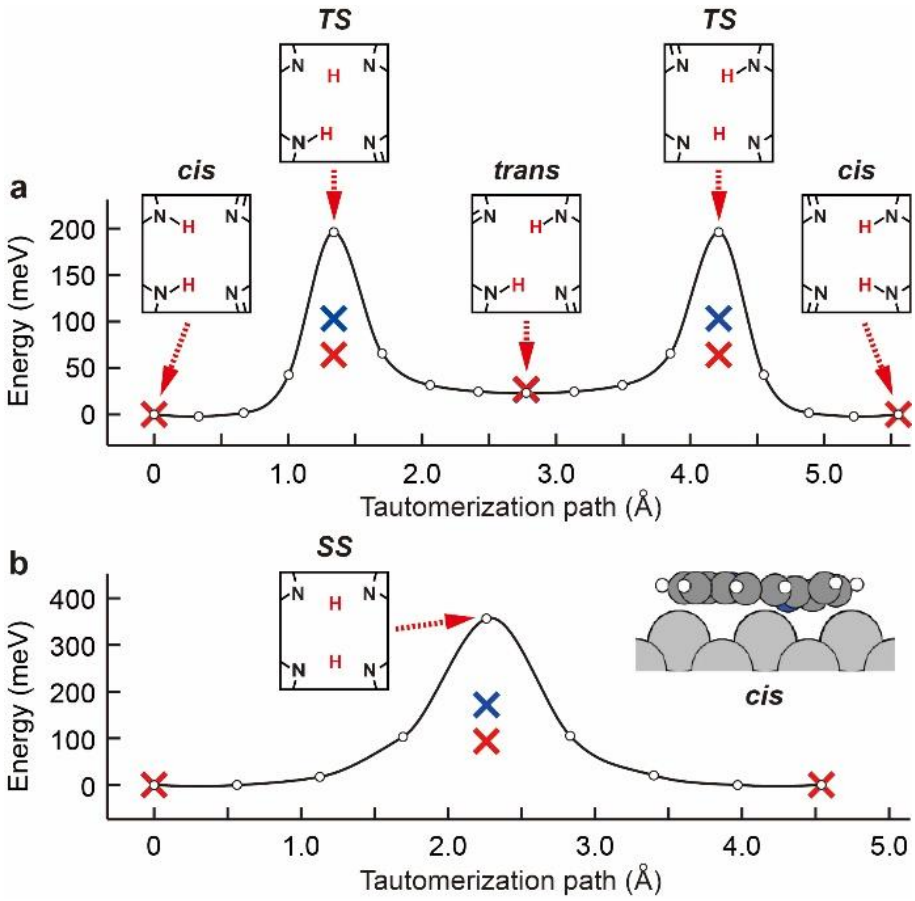

Figure 3. Minimum energy paths (MEPs) of porphycene on Ag(110). (a) and (b) Calculated stepwise and concerted MEPs, respectively. The red and blue crosses represent the zero-point corrected energy for HH- and DD-porphycene, respectively. TS: first-order transition state, SS: second-order saddle point. The inset in **b** shows a side view of the calculated *cis* structure.

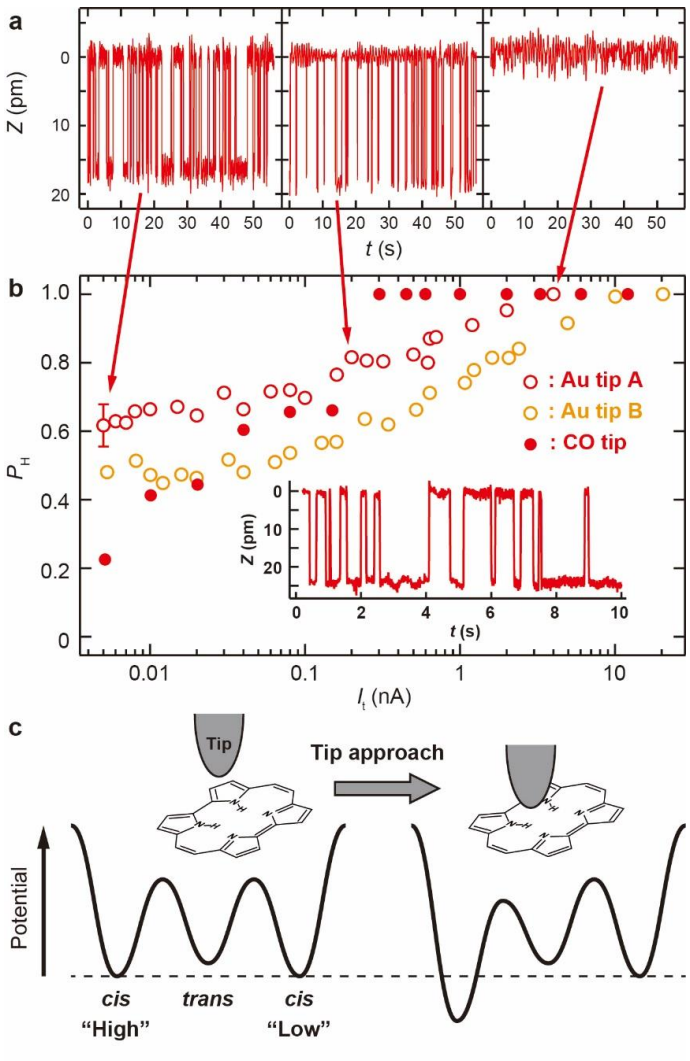

Figure 4. Influence of the tip on the tautomerization dynamics. (a) Tip height traces measured for HH-porphycene at three different gap distances. The lateral tip position was fixed at the position indicated in **Fig. 1d**. (b) Fractional population of the "high" state as a function of a set current (gap distance). The data were obtained for HH-porphycene at 5 K with an Au tip (open circles, at V_{bias} = 20 mV) and with a CO-modified tip (filled circles, at V_{bias} = 10 mV). The inset shows the tip height trace measured for HH-porphycene with the CO-modified tip. (c) Schematic of tautomerization potential deformation caused by the presence of the tip.

Supplementary Information;

Direct observation of double hydrogen transfer via quantum tunnelling in a single porphycene molecule on a Ag(110) surface

Matthias Koch[1], Mats Persson[2], Sylwester Gawinkowski[3], Jacek Waluk[3, 4], Takashi Kumagai*[1]

[1]Department of Physical Chemistry, Fritz-Haber Institute of the Max-Planck Society, Faradayweg 4-6, 14195 Berlin, Germany.

[2]Surface Science Research Centre and Department of Chemistry, University of Liverpool, Liverpool L69 3BX, UK.

[3]Institute of Physical Chemistry, Polish Academy of Sciences, Kasprzaka 44/52, Warsaw 01-224, Poland.

[4]Faculty of Mathematics and Natural Sciences, College of Science, Cardinal Stefan Wyszyński University, Dewajtis 5, 01-815 Warsaw, Poland

*corresponding author: kuma@fhi-berlin.mpg.de

1. Characterization of HH-, HD-, and DD-porphycene on the surface

The deuterated porphycene was prepared by repeated recrystallization of parent HH-porphycene with a mixture of CD_3OD and CD_2Cl_2 solution. Subsequent exposure to air results in partial reprotonation of the inner deuterons. We used the sample that contained partially deuterated species, *i.e.*, HD-porphycene. Usually, NH and ND groups are readily distinguishable by their different stretching frequencies in the IR spectra. This is, however, not the case for porphycene, which shows an extremely broad and structured IR absorption around 2500 cm^{-1} resulting from strong coupling of the stretching mode with other vibrational modes[1]. Practically no absorption is observed in the range of 2000–2500 cm^{-1} for deuterated porphycene in which both inner protons have been replaced by deuterons (DD-porphycene). Because of the lack of characteristic N–H/N–D stretching bands, chemical identification of singly deuterated HD-porphycene is not straightforward and requires specialized techniques, such as electronic spectroscopy of ultra-cold molecules isolated in helium nanodroplets[2]. Recently we demonstrated that porphycene isotopologues are distinguishable on a Cu(110) surface by measuring the conductance and STM-action spectroscopy, as described elsewhere[3]. Based on the statics obtained on Cu(110) the purity of the DD-porphycene sample was determined to be approximately 7:3 of DD- and HD-species.

On the Ag(110) surface, we found two distinct species exhibiting different behavior in tip height traces. In the one case, the trace showed three levels (**Fig. 2d** of the main text), which is attributed to DD-porphycene. In the other case, only two states were observed in the trace but considerably lower rate than that of HH-porphycene (see **Fig. 1** in below). Approximately 30 % of the molecules on Ag(110) upon the same deuterated sample as the above exhibited the latter trace. Therefore, we attributed them

to HD-species.

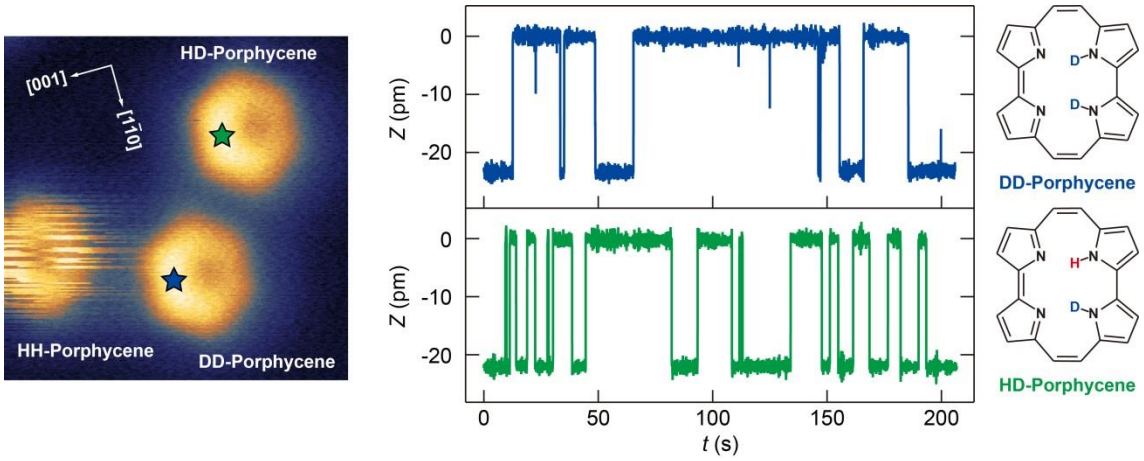

Figure 1 | Trace of tip height (*Z*) measured for DD- and HD-porphycene. The traces were acquired at a set current of 5 pA at V_s = 30 mV. The lateral tip position during the measurement is indicated by the white stars in the STM image.

2. Current (tip height) dependence of HH-, HD-, and DD-porphycene on the surface

In order to prove the negligible influence from tunnelling electrons, an electric field, and/or tip–molecule interaction to the tautomerization for all isotopologues under small tunneling current and bias voltage conditions, we measured the tautomerization rate as a function of the tip–sample distance. As can be seen in **Fig. 2**, the rates stay constant below ~0.1 nA for all species. This result indicates that any STM perturbation does not affect the tautomerization dynamics.

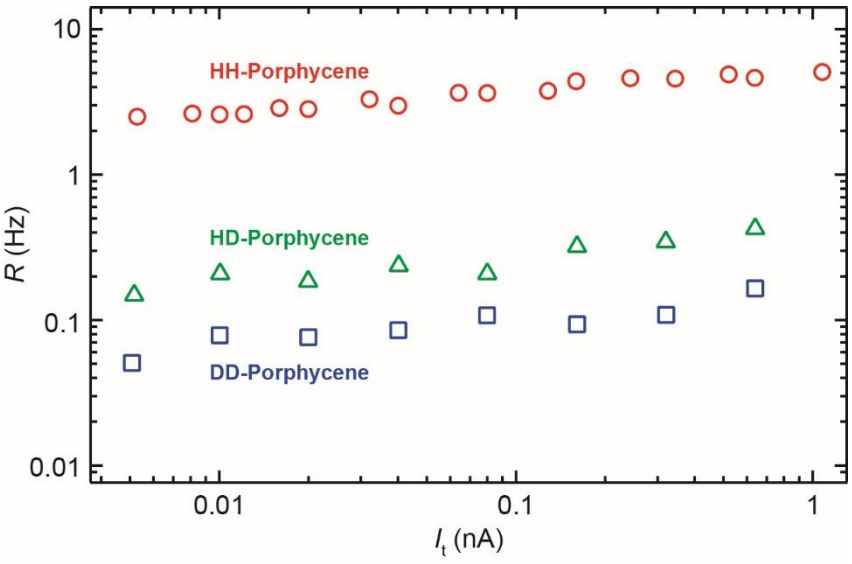

Figure 2 | Current dependence of the tautomerization rates measured at 5 K for HH-, DD-, and HD-porphycene. The rates for the "high" to "low" process are plotted. The bias voltage was fixed to 20 mV during the measurement.

3. Kinetic isotope effects derived from Bell–Limbach tunneling model

In the Bell–Limbach tunneling model the barrier $V(x)$ is approximated by an inverted parabola where the tunneling distance (a), the minimum energy for tunneling to occur (E_m), and the barrier height in the tunneling regime (E_d) are defined (**Fig. 3**)[4]. Em is assumed to be an isotope-independent parameter. The reaction rate constant is derived by applying the tunneling correction (Q_t) to the Arrhenius law to be

$$\mathrm{k} = k_c Q_t = A\exp\left(-\frac{E_d}{k_B T}\right)\int_{E_m}^{\infty}\frac{G(W)}{k_B T}\exp\left(\frac{E_d - W}{k_B T}\right)\mathrm{d}W, \quad (1)$$

where k_c is the rate constant for the classical (over-the-barrier) process, A the pre-exponential factor (the intercept of the Arrhenius plot at high temperature), $G(W)$ the probability of a particle passing through the obstructing barrier at energy W. Eq (1) can be applied to a multiple hydrogen (proton) transfer which involve intermediate states in the reaction pathway.

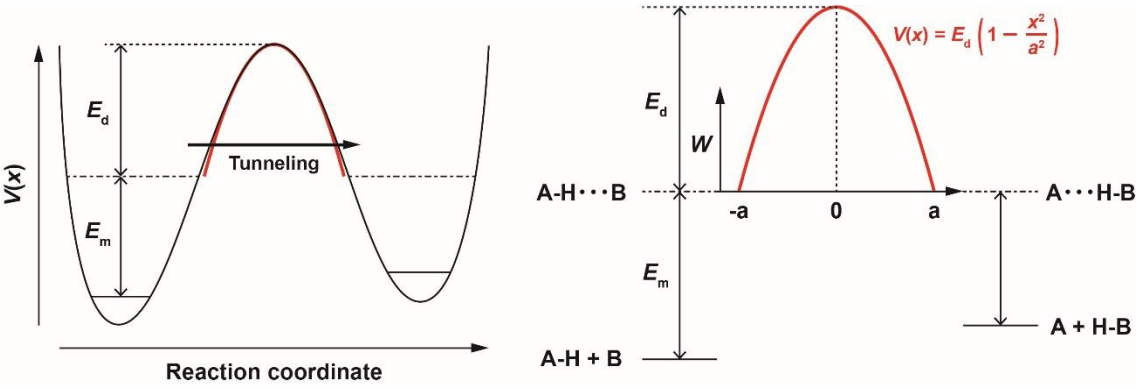

Figure 3 | Scheme of the Bell–Limbach tunneling model. A and B represent heavy atoms and the potential becomes symmetric (degenerate) when A = B.

Figure 4 illustrates a scheme of the stepwise *cis* ↔ *cis* tautomerization, where A and D represent the initial and final states, respectively, and B and C the meta-stable *trans* configuration (*i.e.*, intermediate). Using the steady-state approximation, the rate constant for the whole process, k_{AD}, is given by:

$$k_{AD} = \frac{k_{AB}k_{BD}}{k_{BA} + k_{BD}} + \frac{k_{AC}k_{CD}}{k_{CA} + k_{CD}}. \quad (2)$$

For isotopologues it can be expressed by:

$$k_{AD}^{LL} = \frac{k_{AB}^{LL}k_{BD}^{LL}}{k_{BA}^{LL} + k_{BD}^{LL}} + \frac{k_{AC}^{LL}k_{CD}^{LL}}{k_{CA}^{LL} + k_{CD}^{LL}}, \quad (3)$$

where the superscript, L = H or D. The primary and secondary kinetic isotope effects of each step are given by:

$$P_{ij} = \frac{k_{ij}^{H(L)}}{k_{ij}^{D(L)}} \text{ and } S_{ij} = \frac{k_{ij}^{L(H)}}{k_{ij}^{L(D)}}, \quad (4)$$

where i, j = A, B, C, D and the parentheses represents the bound hydrogen or deuterium. Provided $P_{ij} = P_{ji} = P$ and $S_{ij} = S_{ji} = S$, the following isotopic rate constant can be derived:

$$k_{AD}^{HH} = k_{AB}^{HH}\left(= k_{AC}^{HH}\right), \quad (5)$$

$$k_{\mathrm{AD}}^{\mathrm{HD}} = k_{\mathrm{AD}}^{\mathrm{DH}} = k_{\mathrm{AD}}^{\mathrm{HH}}\left(\frac{2}{S+P}\right) = k_{\mathrm{AD}}^{\mathrm{DD}}\left(\frac{2}{S^{-1}+P^{-1}}\right), \quad (6)$$

$$k_{\mathrm{AD}}^{\mathrm{DD}} = k_{\mathrm{AB}}^{\mathrm{DD}}\left(= k_{\mathrm{AC}}^{\mathrm{DD}}\right) = k_{\mathrm{AD}}^{\mathrm{HH}} P^{-1} S^{-1}. \quad (7)$$

When secondary isotope effects are absent, Eqs. (4)–(6) become

$$k_{\mathrm{AD}}^{\mathrm{HH}} = k_{\mathrm{AB}}^{\mathrm{HH}}\left(= k_{\mathrm{AC}}^{\mathrm{HH}}\right), \quad (8)$$

$$k_{\mathrm{AD}}^{\mathrm{HD}} = k_{\mathrm{AD}}^{\mathrm{DH}} = k_{\mathrm{AD}}^{\mathrm{HH}}\left(\frac{2}{1+P}\right) = k_{\mathrm{AD}}^{\mathrm{DD}}\left(\frac{2}{1+P^{-1}}\right), \quad (9)$$

$$k_{\mathrm{AD}}^{\mathrm{DD}} = k_{\mathrm{AB}}^{\mathrm{DD}}\left(= k_{\mathrm{AC}}^{\mathrm{DD}}\right) = k_{\mathrm{AD}}^{\mathrm{HH}} P^{-1}. \quad (10)$$

The notations can be simplified to k^{LL} and according to Eq. (3) $P = P^{\mathrm{HH}}/P^{\mathrm{DD}}$, leading to

$$k^{\mathrm{HD}} = \frac{2k^{\mathrm{HH}}}{1 + k^{\mathrm{HH}}/k^{\mathrm{DD}}} = \frac{2k^{\mathrm{HH}}}{1 + k^{\mathrm{DD}}/k^{\mathrm{HH}}}, \quad (11)$$

$$k^{\mathrm{DD}} = k^{\mathrm{HH}} P^{-1}. \quad (12)$$

At low temperatures where tunneling governs the reaction, thus $k^{\mathrm{HH}} \gg k^{\mathrm{DD}}$ we obtain $k^{\mathrm{HD}} \cong 2k^{\mathrm{DD}}$.

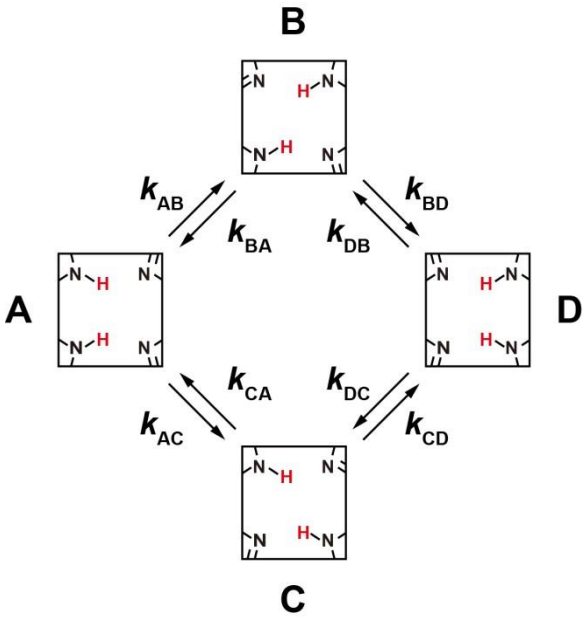

Figure 4 | Scheme of the stepwise *cis* ↔ *cis* tautomerization.

The concerted mechanism is characterized by a single barrier. In the tunneling model

described above, the isotope sensitive tunneling distance depends on the barrier height and is given by

$$2a^{\mathrm{HD}} = 2a^{\mathrm{HH}}\sqrt{\frac{E_{\mathrm{d}}^{\mathrm{HD}}}{E_{\mathrm{d}}^{\mathrm{HH}}}}, 2a^{\mathrm{DD}} = 2a^{\mathrm{HH}}\sqrt{\frac{E_{\mathrm{d}}^{\mathrm{DD}}}{E_{\mathrm{d}}^{\mathrm{HH}}}}, \quad (13)$$

Assuming that replacement of each hydrogen by deuterium leads to the same increase in the barrier, thus

$$E_{\mathrm{d}}^{\mathrm{HD}} = E_{\mathrm{d}}^{\mathrm{HH}} + \Delta\varepsilon, E_{\mathrm{d}}^{\mathrm{DD}} = E_{\mathrm{d}}^{\mathrm{HH}} + 2\Delta\varepsilon, \quad (14)$$

we could derive the rule of the geometric mean for the kinetic isotope effect at high temperatures where the classical process is dominant

$$\frac{k^{\mathrm{HH}}}{k^{\mathrm{HD}}} = \frac{k^{\mathrm{HD}}}{k^{\mathrm{DD}}}. \quad (15)$$

However, it has been found that this rule could also be maintained in good agreement even at low-temperatures, *i.e.*, in the tunneling regime[5]. This implies that the barrier height, the tunneling distance, and the tunneling mass correspond practically to the arithmetic mean of the HH and DD transfer.

4. Details of the density functional theory (DFT) calculations

The DFT calculations of the adsorption of the porphycene adsorption on Ag(110) were done in same manner as in our previous calculations for the adsorption on Cu(110)[4]. These calculations were carried out using the Vienna ab-initio simulation program (VASP)[5]. The electron-ion core interactions and the exchange-correlation effects were treated using the Projector Augmented Wave (PAW) method[6] and the optB86B version of the van der Waals density functional[7-10] respectively. The plane-wave cut-off was 400 eV. The Ag(110) surface was represented in a super-cell by a four layer slab with a 4×6 surface unit cell and a 20 Å vacuum region. A 2×2×1 grid was used in the k-point

sampling. The structures were relaxed until all forces were less than 0.01 eV/Å, with the bottom two Ag layers kept fixed throughout the geometry optimization at the calculated lattice constant of 4.10 Å. Top views of the calculated structures of the *cis* and *trans* configurations of Ag(110) and Cu(110) are shown in Fig. S2a and b. A measure of the buckling of the adsorbed molecule is provided by the relative height, Δh_B, of the imine and amine nitrogen atoms and is shown in Table 1.

The vibrational energies of the adsorbed molecule on a rigid substrate lattice was calculated by diagonalising the dynamical matrix which was obtained by finite differences of the calculated forces at symmetric ionic displacements of 0.02 Å. The minimum energy paths (MEPs) and the reaction barriers were calculated using the nudged elastic band (NEB) method[11-12].

	Ag(110)				Cu(110)			
	cis	TS_{SP}	TS_{CP}	*trans*	*cis*	TS_{SM}	TS_{CM}	*trans*
Δh_B (Å)	0.44			0.18	0.61			0.32
E (eV)	0.0	0.196	0.358	0.023	0.0	0.342	0.628	0.184
$\tilde{E}$ (eV)	0.0	0.064 (0.103)	0.094 (0.172)	0.027 (0.026)	0.0	0.203 (0.243)	0.352 (0.432)	0.184 (0.184)
$\hbar\omega$ (eV)		0.137	0.117,0.136 (0.083,0.096)			0.128	0.124,0.138 (0.088,0.098)	

Table 1 | Calculated bucklings of the molecular skeleton, Δh_B, potential energies, E, and zero-point-energy corrected energies, $\tilde{E}$, and imaginary vibrational energies, $i\hbar\omega$. The transition structures for the step-wise and concerted MEPs are denoted by TS_{SP} and TS_{SP}, respectively. The energies are referenced with respect to the *cis*

configuration. The values within the parenthesis are the corresponding values for the fully deuterated inner H atoms (HH- and DD-porphycene, respectively).

5. Minimum energy paths (MEPs) of the stepwise and concerted hydrogen transfer

As done before for Cu(110)[4], the MEP for the step-wise mechanism (Fig. 4f of the main text) was obtained by constraining the path to pass through one of the two intermediate, degenerate *trans* configurations, whereas the concerted path was obtained by enforcing reflection symmetry through the vertical mirror plane of the adsorbed molecule in the *cis* configurations.

As shown in Fig. 3a of the main text for Ag(110) and Fig. S2a for Cu(110), the step-wise path is symmetric with respect to the *trans* configuration and exhibits two equivalent transition structures (first-order saddle points). As shown in Fig. 3b and Fig. S2a, the concerted path is also symmetric with respect to the initial and final *cis* configurations but with a single transition structure (second-order saddle-point). Furthermore, the relatively large path length between the initial and final configuration indicates that there are substantial movements of not just the inner H atoms during the tautomerization.

The potential energies, *E*, of the *cis* and *trans* configurations and the transition structures for the stepwise and concerted paths are listed in Table S1. Here we have also listed the zero-point-energy corrected energies for HH-porphycene and DD-porphycene. These latter energies was obtained as, $\tilde{E}(\mathrm{conf}) = E(\mathrm{conf}) + E_{\mathrm{ZPE}}(\mathrm{conf}) - E_{\mathrm{ZPE}}(cis)$, where "conf" is the configuration and E_{ZPE} is the zero-point energy as obtained from the calculated (real) vibrational energies when keeping all atoms except the inner hydrogen or deuterium atoms fixed. These energies changes with at most a couple of meV when

including the nitrogen atoms. In Table S2, we have also listed the calculated imaginary vibrational energies $i\hbar\omega$ at the transition structures.

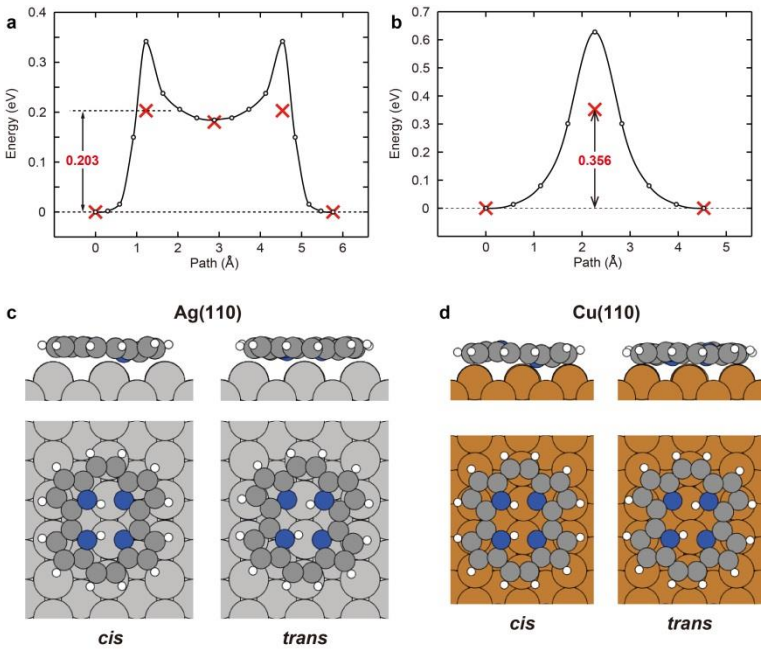

Figure 3 | MEPs and calculated structures. a and b, MEPs for the stepwise and concerted transfer, respectively, on a Cu(110) surface. **c and d**, calculated structures on Ag(110) and Cu(110), respectively. The larger buckling of the molecular skeleton occurs on Cu(110) (see, Table S1).

References

[1] S. Gawinkowski, Ł. Walewski, A. Vdovin, A. Slenczka, S. Rols, M. R. Johnson, B. Lesyngef and J. Waluk, Vibrations and hydrogen bonding in porphycene. *Phys. Chem. Chem. Phys.* **14**, 5489–5503 (2012).

[2] A. Vdovin, J. Waluk, B. Dick and A. Slenczka, Mode-Selective Promotion and Isotope Effects of Concerted Double-Hydrogen Tunnelling in Porphycene Embedded in Superfluid Helium Nanodroplets. *Chem. Phys. Chem.* **10**, 761–765 (2009).

[3] T. Kumagai, S. Gawinkowski, J. Waluk, Tautomerization of porphycene isotopologues on a Cu(110) surface. *Submitted*.

[4] J. N. Ladenthin, T. Frederiksen, M. Persson, J. C. Sharp, S. Gawinkowski, J. Waluk and T. Kumagai, Force-induced tautomerization in a single molecule, J. N. Ladenthin, T. Frederiksen, M. Persson, J. C. Sharp, S. Gawinkowski, J. Waluk and T. Kumagai, Nature Chemistry **8**, 935 (2016)

[5] Kresse, G. & Furthmüller, J. Efficient iterative schemes for ab initio total-energy calculations using a plane-wave basis set. Phys. Rev. B **54**, 11169 (1996).

[6] Kresse, G. & Joubert, D. From ultrasoft pseudopotentials to the projector augmented-wave method. Phys. Rev. B **59**, 1758 (1999).

[7] Dion, M., Rydberg, H., Schröder, E., Langreth, D. C. & Lundqvist, B. I. Van der Waals Density Functional for General Geometries. Phys. Rev. Lett. **92**, 246401 (2004).

[8] Román-Pérez, G. & Soler, J. M. Efficient Implementation of a van der Waals Density Functional: Application to Double-Wall Carbon Nanotubes. Phys. Rev. Lett. **103**, 096102 (2009).

[9] Klimeš, J., Bowler, D. R. & Michaelides, A. Chemical accuracy for the van der Waals density functional. J. Phys. Cond. Matt. **22**, 022201 (2010).

[10] Klimeš, J., Bowler, D. R. & Michaelides, A. Van der Waals density functionals applied to solids. Phys. Rev. B **83**, 195131 (2011).

[11] Mills, G., Jónsson, H. & Schenter, G. K. Reversible work transition state theory: application to dissociative adsorption of hydrogen. Surf. Sci. **324**, 305–337 (1995).

[12] Henkelman, G., Uberuaga & B. P., Jónsson, H. A climbing image nudged elastic band method for finding saddle points and minimum energy paths. J. Chem. Phys. **113**, 9901–9904 (2000).

[4] H. H. Limbach, Single and multiple hydrogen/deuterium transfer reactions in liquids and solids, in Hydrogen Transfer Reactions , ed. J. T. Hynes, J. Klinman, H. H. Limbach and R. L. Schowen, Wiley-VCH, Weinheim, 2007, vol. 1 & 2, ch. 6, pp. 135–221.

[5] Lopez, J. M., Männle, F., Wawer, I., Buntkowsky, G. and Limbach, H.-H. NMR studies of double proton transfer in hydrogen bonded cyclic *N*,*N*′-diarylformamidine dimers: conformational control, kinetic HH/HD/DD isotope effects and tunneling. *Phys. Chem. Chem. Phys.* **9**, 4498–4513 (2007).